Absorption of sound by porous layers with embedded periodic arrays of resonant inclusions

Clément Lagarrigue, Jean-Philippe Groby, Vincent Tournat, Olivier Dazel,
Olga Umnova

Absorption of sound by porous layers with embedded periodic arrays of resonant inclusions

C. Lagarrigue,[a] J. P. Groby, V. Tournat, and O. Dazel
LUNAM Université, Université du Maine, CNRS, LAUM UMR-CNRS 6613 (Laboratoire d'Acoustique de l'Université du Maine), Avenue O. Messiaen, 72085 Le Mans, France

O. Umnova
Acoustics Research Centre, University of Salford, Salford, Greater Manchester, M5 4WT, United Kingdom

The aim of this work is to design a layer of porous material with a high value of the absorption coefficient in a wide range of frequencies. It is shown that low frequency performance can be significantly improved by embedding periodically arranged resonant inclusions (slotted cylinders) into the porous matrix. The dissipation of the acoustic energy in a porous material due to viscous and thermal losses inside the pores is enhanced by the low frequency resonances of the inclusions and energy trapping between the inclusion and the rigid backing. A parametric study is performed in order to determine the influence of the geometry and the arrangement of the inclusions embedded in a porous layer on the absorption coefficient. The experiments confirm that low frequency absorption coefficient of a composite material is significantly higher than that of the porous layer without the inclusions.

I. INTRODUCTION

Traditionally, porous materials are used for noise reduction. However, when used with rigid backing, porous absorbers are efficient only if distance from their surface to the wall exceeds a quarter of the sound wavelength. This results in layers that are too thick if absorption of low frequency sound is required. The usual way to solve this problem is to use multi-layered[1] structures. The purpose of the present study is to investigate an alternative to multi-layering by embedding a periodic set of resonant inclusions which are small compared to sound wavelength in an otherwise macroscopically homogeneous, relatively thin and light porous layer. In the following, the resonant inclusions with a split ring (SR) shape cross section are considered. The inclusions and the porous skeleton are assumed motionless. The configuration results in a diffraction grating due to the inclusion periodicity.[2] The influence of a volume heterogeneity on the absorption and transmission coefficients of a porous layer without rigid backing was previously investigated using the multipole method. A periodic set of high-contrast inclusions in a macroscopically homogeneous porous layer was considered.[3] In that case, the sizes of the inclusions were comparable to sound wavelength in porous medium. It was shown that the presence of the inclusions leads to either an increase in the absorption coefficient as in the case of one row of inclusions, or to a total absorption peak, as in the case of several rows set of inclusions (phononic crystal). The changes in the absorption coefficient were explained by mode excitation due to the presence of periodically arranged inclusions, which leads to energy entrapment. Furthermore, a "trapped mode" is excited due to periodicity when the structure is placed against a rigid boundary[2] that increases the absorption coefficient for frequencies below the quarter-wavelength resonance of the porous layer. Trapped modes were previously studied in waveguides[4] or periodic structures.[5] Here, the modification of the absorption coefficient due to a periodic arrangement of resonant inclusions embedded into a porous layer glued to a rigid backing (see Fig. 1) is investigated theoretically, numerically, and experimentally.

The periodicity allows the energy entrapment below the quarter-wavelength resonance. Bragg's interference is significant at higher frequencies and leads to the decrease of the absorption coefficient when wavelength in the porous layer is comparable to four times the distance between the center of the inclusion and the wall. At last, the resonances of the inclusions can increase the absorption coefficient at very low frequencies. The investigation is focused on two phenomena, which are the inclusion resonance and the trapped modes.

II. FORMULATION OF THE PROBLEM

A. Description of the configuration

A geometry of the two-dimensional (2D) problem considered in this work is shown in Fig. 1. The porous material is assumed to have rigid frame and, consequently, can be described as a homogeneous effective fluid with effective density, ρ_1, and bulk modulus, χ_1, defined as (time convention in the form of $e^{-i\omega t}$ is assumed)

$$\rho_1 = \frac{\rho_0 \alpha_\infty}{\phi} \left(1 + \frac{2\pi\nu_b}{-i\omega} \sqrt{1 + \frac{-i\omega}{2\pi\nu_c}} \right), \qquad (1)$$

with

---
[a]Author to whom correspondence should be addressed. Electronic mail: clement.lagarrigue.etu@univ-lemans.fr
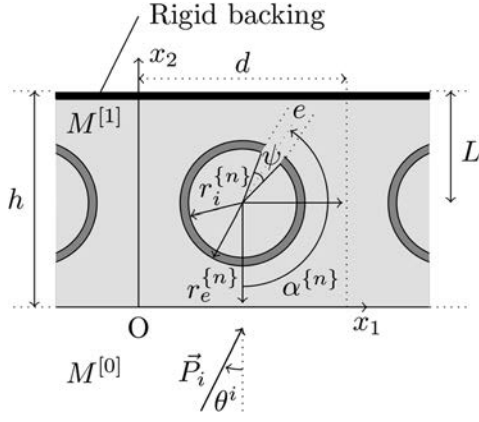
FIG. 1. Geometry of the problem.

$$2\pi\nu_b = \frac{\sigma\phi}{\rho_0\alpha_\infty}, \quad 2\pi\nu_c = \frac{\sigma^2\phi^2\Lambda^2}{4\alpha_\infty^2\rho_0\eta}, \tag{2}$$

and

$$\chi_1 = \frac{\gamma P_0/\phi}{\gamma - (\gamma-1)\left(1 + \dfrac{2\pi\nu_b'}{-i\omega}\sqrt{1 + \dfrac{-i\omega}{2\pi\nu_c'}}\right)^{-1}}, \tag{3}$$

with

$$2\pi\nu_b' = \frac{\eta\phi}{\rho_0 k_0'\alpha_\infty\mathrm{Pr}}, \quad 2\pi\nu_c' = \frac{\eta\Lambda'^2\phi^2}{4\rho_0 k_0'^2\alpha_\infty^2\mathrm{Pr}}, \tag{4}$$

where the Johnson et al.[6] model is used for the effective density, ρ_1, and the Champoux and Allard[7] model is used for the effective bulk modulus, χ_1. Here, η is the dynamic air viscosity, ρ_0 is air density, $\mathrm{Pr} = \eta c_p/\kappa$ is the Prandtl number, c_p is air heat capacity under constant pressure, κ is thermal conduction coefficient of air, γ is the adiabatic constant, P_0 is the static ambient pressure, σ is the material flow resistivity, α_∞ is the tortuosity, ϕ is the porosity, and Λ and Λ' are characteristic viscous and thermal lengths, respectively. A value $k_0' = \phi\Lambda'^2/8$ has been used for the thermal permeability.

The medium, $M^{[0]}$, is air. The normal displacement and the pressure are continuous at the interface between the porous material and the air. Pressure and displacement variations in the plane wave propagating in rigid porous material are described by the following equations:

$$-p = \chi_1\nabla u_{\mathrm{eq}}, \quad -\omega^2\rho_1 u_{\mathrm{eq}} = -\nabla p, \tag{5}$$

with $u_{\mathrm{eq}} = \phi u_f$, and u_f is the displacement of the fluid in the pores.

The inclusion boundaries are considered infinitely rigid (Neumann type boundary condition on the interface porous medium/inclusion) and the medium inside the resonant inclusions is the same porous material as the one outside. The position of the slit of the inclusion is defined by the angle, $\alpha^{\{n\}}$. The inclusion is characterized by its outer radius, r_e, the opening width, e, the thickness, $H = r_e^{\{n\}} - r_i^{\{n\}}$, and ψ, the aperture. Thus, the layer is macroscopically

inhomogeneous, with heterogeneity being periodic in the x_1 direction with period d. In all simulations the rigid backing (Neumann type boundary condition) is placed at the top of the inclusion at $x_2 = h$. The numerical simulations have been performed using a finite element method (FEM) developed and validated in the article by Allard et al.[8] The mesh is created by using FreeFem++ and the problem is solved by implementing a Johnson-Champoux-Allard model in an in-house Fortran code specially written for calculating the acoustic response of 2D periodic media. Linear finite elements are used to approximate the pressure inside the unit cell, thereby leading to a discretized problem of 1128 elements and 714 nodes. The periodicity boundary conditions (the Floquet-Bloch conditions) are applied on both sides of the discretized domain. For this to be correctly implemented, these two sides are discretized with similar nodes, i.e., identical x_2 coordinates.

The initial unit cell is a square of side length 2 cm. The porous material has the characteristics of Fireflex (Recticel, Belgium) backed by a rigid plate. Fireflex is a polyether based foam commercialized for its good fire resistant properties and acoustic performance. The parameters used for this porous layers have been determined by classical methods in ATF, KU Leuven, Belgium (Table I). Calculations are performed by considering an incident plane wave that propagates from the bottom of the cell along the x_2 axis.

III. RESONANCE FREQUENCY OF A SPLIT RING AND A SCATTERING MODEL

In this section the resonance frequency of a single SR inclusion is calculated in both air and in porous material. Moreover, the case of a SR placed close to a rigid boundary is considered and the dependence of the resonance frequency on the distance to the wall and slit orientation is studied. The approach to modeling sound scattering by periodically arranged SRs is described at the end of the section.

A. Resonance frequency of a split ring in air

SR is a 2D Helmholtz resonator. The resonance frequency of this structure has been calculated in, for example, Norris and Wickham[9] and Krynkin et al.[10] Here the calculations are briefly outlined to emphasize the influence of the opening radiation impedance on the resonance frequency. The radiation impedance is defined as the ratio of the average radiated sound pressure to the particle velocity at the outer surface of the opening. This influence is important when the resonance frequency of a SR placed close to the rigid boundary is calculated. The pressure, p, in air satisfies the Helmholtz equation, which in cylindrical coordinates, r and θ, is

TABLE I. Parameters of the porous foam [Fireflex (Recticel, Belgium)] used in FEM and semi-analytical calculations.

ϕ	α_∞	Λ (μm)	Λ' (μm)	σ (N s m^{-4})
0.95	1.42	180	360	8900

TABLE II. Dimensions for the configuration C1. These geometric values are defined Fig. 1.

C1	r_i (cm)	r_e (cm)	d (cm)	e (cm)	h (cm)	l (cm)
	0.7	0.744	2	0.14	2	1

$$\left(\frac{1}{r}\frac{\partial}{\partial r}\left(r\frac{\partial}{\partial r}\right)+\frac{1}{r^2}\frac{\partial^2}{\partial\theta^2}\right)p + k^2 p = 0, \qquad (6)$$

where $k = \omega/c$ is the wavenumber in air. The pressure, p_i, and the r-component of particle velocity, v_i, inside the circular cavity are

$$p_i = \sum_{n=-\infty}^{\infty} A_n J_n(kr) e^{in\theta}, \qquad (7)$$

$$v_i = \frac{k}{i\omega\rho_0}\sum_{n=-\infty}^{\infty} A_n J_n'(kr) e^{in\theta}. \qquad (8)$$

Here and everywhere in this section the derivatives of Bessel functions are taken with respect to their arguments. Following the approach described in Krynkin *et al.*,[10] a piston-like motion inside the slit $r_i \leq r \leq r_i + H$, $-\psi/2 \leq \theta \leq \psi/2$ is assumed, with pressure, p_h, and particle velocity, v_h, expressed as

$$p_h = Ce^{ikr} + Be^{-ikr}, \qquad (9)$$

$$v_h = \frac{1}{\rho_0 c}(Ce^{ikr} - Be^{-ikr}). \qquad (10)$$

This approximation is valid if both resonator wall thickness, H, and the slit width, $e = \psi r_i$, are small compared to the wavelength ($ke \ll 1$, $kH \ll 1$) and the radius r_i ($e/r_i \ll 1$, $H/r_i \ll 1$). The coefficients A_n, B, and C are found from the following boundary conditions. First, the boundary condition for the particle velocity on the SR inner surface is

$$v_i(r = r_i, \theta) = v_h(r = r_i)(\mathbf{H}(\theta + \psi/2) - \mathbf{H}(\theta - \psi/2)), \qquad (11)$$

where $\mathbf{H}$ is a Heaviside step function. Combined with orthogonality conditions, this leads to the following expressions for the coefficients A_n:

$$A_0 = \frac{i\psi}{2\pi J_0'(kr_i)}(Ce^{ikr_i} - Be^{-ikr_i}), \qquad (12)$$

$$A_n = \frac{i}{\pi J_n'(kr_i)}(Ce^{ikr_i} - Be^{-ikr_i})\frac{\sin\left(\frac{n\psi}{2}\right)}{n}, \qquad (13)$$

where $n \geq 1$ and $A_{-n} = A_n$. Second, pressure, p_i, averaged over the opening, i.e., $\bar{p}_i = (1/\psi)\int_{-\psi/2}^{\psi/2} p_i(r = r_i, \theta)\,d\theta$ should be equal to that on the slit inner surface. From Eqs. (7), (12), and (13)

$$\bar{p}_i = (Ce^{ikr_i} - Be^{-ikr_i})$$
$$\times\left(\frac{i\psi}{2\pi}\frac{J_0(kr_i)}{J_0'(kr_i)} + \frac{4i}{\pi\psi}\sum_{n=1}^{\infty}\frac{J_n(kr_i)}{J_n'(kr_i)}\frac{\sin^2\left(\frac{n\psi}{2}\right)}{n^2}\right). \qquad (14)$$

This has to satisfy the following condition:

$$\bar{p}_i = Ce^{ikr_i} + Be^{-ikr_i}. \qquad (15)$$

Finally, at the outer surface of the opening at $r = r_e = r_i + H$, the ratio of p_h and v_h is equal to the slit radiation impedance, $\bar{z}$,

$$\rho_0 c\frac{Ce^{ikr_e} + Be^{-ikr_e}}{Ce^{ikr_e} - Be^{-ikr_e}} = \bar{z}. \qquad (16)$$

Combining this with Eqs. (14) and (15) and leaving only the leading terms in the expansion of $\tan(kH)$, the following characteristic equation is obtained:

$$\frac{\bar{z}}{\rho_0 c} = \frac{Q + i(kH)}{iQ(kH) + 1}, \qquad (17)$$

where

$$Q = \frac{i\psi}{2\pi}\frac{J_0(kr_i)}{J_0'(kr_i)} + \frac{4i}{\pi\psi}\sum_{n=1}^{\infty}\frac{J_n(kr_i)}{J_n'(kr_i)}\frac{\sin^2\left(\frac{n\psi}{2}\right)}{n^2}. \qquad (18)$$

Resonance frequencies of a SR resonator are the solutions of characteristic Eq. (17) and, hence, depend on the radiation impedance of the opening. Now, assuming $kr_i = O(\beta)$, $kH = O(\beta^2)$, $\delta/H = O(1)$ (end correction δ is defined below), where β is a small parameter, and leaving only the leading terms in the expansions in Eqs. (17) and (18),

$$\frac{J_0(kr_i)}{J_0'(kr_i)} = -\frac{2}{kr_i} + O(\beta), \quad \frac{J_n(kr_i)}{J_n'(kr_i)} = \frac{kr_i}{n} + O(\beta^3), \qquad (19)$$

the following equation can be obtained for the resonance frequency, f_r, of the SR resonator

$$\bar{Z} = -\frac{-ie}{\pi k_r r_i^2} + ik_r(H + \delta), \qquad (20)$$

where $k_r = 2\pi f_r/c$, $\bar{Z} = \bar{z}/\rho_0 c$ is the normalized radiation impedance of the slit, and the inner end correction, δ, is

$$\delta = e\frac{4}{\pi\psi^2}\sum_{n=1}^{\infty}\frac{\sin^2\left(\frac{n\psi}{2}\right)}{n^3}. \qquad (21)$$

Radiation impedance of the slit, $\bar{Z}$, depends on the resonator surroundings. In the simplest case when the resonator is placed in an unbounded homogeneous medium (free field), it can be calculated in the following way. Piston motion approximation (9), (10) assumes that particle velocity on the outer slit surface is angle independent and is equal to $v_0 = v_h(r = r_e)$. According to Shenderov,[11] pressure at the point with coordinates (r, θ) (coordinate system is centered at the cylinder) generated by an arbitrary velocity distribution, $v(\theta)$, on the surface of a cylinder with radius, r_e, can be calculated as

$$p(r, \theta) = -\frac{i\omega\rho_0}{4\pi}\int_0^{2\pi} v(\theta_0)G(r, r_e, \theta, \theta_0)\,d\theta_0, \qquad (22)$$

3

where

$$G(r, r_e, \theta, \theta_0) = -\frac{2}{kr_e} \sum_{n=-\infty}^{\infty} \frac{H_n^{(1)}(kr)}{H_n^{(1)'}(kr_e)} e^{in(\theta-\theta_0)} \qquad (23)$$

is the Green's function of a cylinder in a free field chosen so that $\partial G/\partial r = 0$ on the cylinder surface and $H_n^{(1)}$ is the Hankel function of the first kind. As the velocity is uniformly distributed over the slit and zero everywhere else on the SR surface, the ratio of pressure [Eq. (22)] averaged over the slit to the velocity, v_0, gives the following expression for the normalized radiation impedance $\bar{Z} = (\int_{-\psi/2}^{\psi/2} p(r_e, \theta) \, d\theta)/\psi v_0 \rho_0 c$:

$$\bar{Z} = \frac{2i}{\pi\psi} \left(\frac{\psi^2}{4} \frac{H_0^{(1)}(kr_e)}{H_0^{(1)'}(kr_e)} + 2\sum_{n=1}^{\infty} \frac{H_n^{(1)}(kr_e)}{H_n^{(1)'}(kr_e)} \frac{\sin^2\left(\frac{n\psi}{2}\right)}{n^2} \right). \qquad (24)$$

As before, a small resonator with $kr_e = O(\beta)$, $\psi/2\pi = O(\beta^2)$ is considered. So leaving only the leading order terms in the following expansions:

$$\frac{H_0^{(1)}(kr_e)}{H_0^{(1)'}(kr_e)} = O(\beta \log(\beta)), \quad \frac{H_n^{(1)}(kr_e)}{H_n^{(1)'}(kr_e)} = -\frac{kr_e}{n} + O(\beta^3). \qquad (25)$$

Equation (24) is reduced to

$$\bar{Z} = -ik\delta, \qquad (26)$$

where δ is defined by Eq. (21). This means that for a small resonator in the free field, the outer end correction is equal to the inner one. Substitution of Eq. (26) in characteristic equation (20) leads to the following expression for the resonance frequency of SR in air:

$$f_r = \frac{k_r c}{2\pi} = \frac{c}{2\pi} \sqrt{\frac{e}{\pi r_i^2 (H + 2\delta)}}. \qquad (27)$$

B. Resonance frequency of a split ring in the presence of a rigid boundary

The presence of a rigid boundary close to the SR changes the radiation impedance, $\bar{Z}$, of its slit and so affects the resonance frequency. To derive the radiation impedance, consider a SR placed at a distance, L, from the rigid boundary. The slit orientation relative to the wall is described by angle $\phi = \pi - \alpha^{\{n\}}$, where angle $\alpha^{\{n\}}$ is shown in Fig. 1. The positions of the SR and its image relative to the rigid boundary are shown in Fig. 2.

The pressure field outside the SR and its image is

$$p = \sum_{n=-\infty}^{\infty} a_n H_n^{(1)}(kr) e^{in\theta} + \sum_{n=-\infty}^{\infty} a_n H_n^{(1)}(kr') e^{in\theta'}, \qquad (28)$$

where (r, θ) are polar coordinates of the observation point in the coordinate system centered at the SR, while (r', θ') are coordinates in the system centered at its image. It is easy to
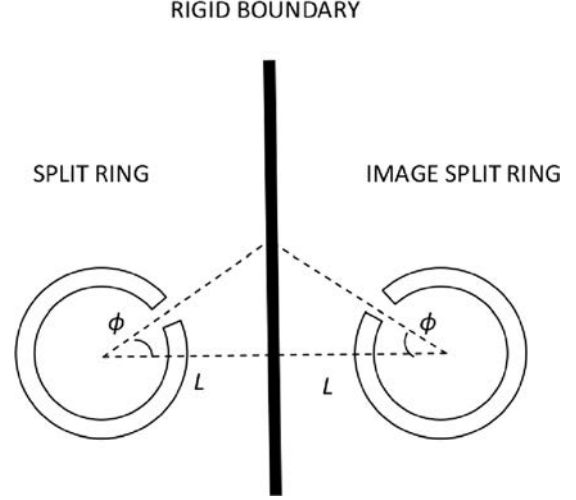

FIG. 2. Split ring resonator placed against the rigid boundary and its image.

show that normal derivative of p defined by Eq. (28) is zero at the wall. Applying Graf's addition theorem,[12] Eq. (28) is transformed to

$$p = \sum_{n=-\infty}^{\infty} \left[a_n H_n^{(1)}(kr) + J_n(kr) \sum_{m=-\infty}^{\infty} a_m H_{m+n}^{(1)}(2kL) \right] e^{in\theta}. \qquad (29)$$

The radial component of the particle velocity is

$$v_r = \frac{1}{i\rho_0 c} \sum_{n=-\infty}^{\infty} \left[a_n H_n^{(1)'}(kr) + J_n'(kr) \sum_{m=-\infty}^{\infty} a_m H_{m+n}^{(1)}(2kL) \right] e^{in\theta}. \qquad (30)$$

The pressure averaged over the opening $r = r_e$, $\phi + \psi/2 \leq \theta \leq \phi - \psi/2$ is

$$\bar{p} = \sum_{n=-\infty}^{\infty} \left[a_n H_n^{(1)}(kr) + J_n(kr) \sum_{m=-\infty}^{\infty} a_m H_{m+n}^{(1)}(2kL) \right] q(n), \qquad (31)$$

where

$$q(n) = \frac{\sin\left(\frac{n\psi}{2}\right)}{\frac{n\psi}{2}}, \quad n \neq 0, \qquad (32)$$

and

$$q(0) = 1. \qquad (33)$$

A uniform velocity, v_0, at the slit surface is assumed as before and the following boundary condition for v_r is applied on the surface of the SR:

$$v_r(r = r_e, \theta) = v_0(\mathbf{H}(\theta - \phi + \psi/2) - \mathbf{H}(\theta - \phi - \psi/2)), \qquad (34)$$

which is similar to Eq. (11). Using orthogonality conditions, the following infinite system of equations for coefficients $b_n = e^{in\phi} a_n H_n^{(1)\prime}(kr_e)/(i\rho_0 c v_0)$ is derived:

$$b_n + J_n'(kr_e) \sum_{m=-\infty}^{\infty} b_m e^{i(n-m)\phi} \frac{H_{m+n}^{(1)}(2kL)}{H_m^{(1)\prime}(kr_e)} = \frac{\psi q(n)}{2\pi}. \quad (35)$$

In terms of coefficients b_n, the normalized radiation impedance of the slit in the presence of wall, $\bar{Z}_w$, is expressed as

$$\bar{Z}_w = i \sum_{n=-\infty}^{\infty} \left[b_n \frac{H_n^{(1)}(kr_e)}{H_n^{(1)\prime}(kr_e)} \right.$$
$$\left. + J_n(kr_e) \sum_{m=-\infty}^{\infty} b_m e^{i(n-m)\phi} \frac{H_{m+n}^{(1)}(2kL)}{H_m^{(1)\prime}(kr_e)} \right] q(n). \quad (36)$$

The next step is to use Bessel and Hankel function expansions in Eqs. (35) and (36) assuming $kr_e = O(\beta)$ and $2kL = O(\beta)$ and leaving only the leading terms. In addition to Eq. (25), the following expansions have been used $(m, n \neq 0)$:

$$J_0(kr_e) = 1 + O(\beta^2), \quad (37)$$

$$J'_0(kr_e) = -\frac{kr_e}{2} + O(\beta^3), \quad (38)$$

$$J_n(kr_e) = \frac{(kr_e)^n}{2^n n!} + O(\beta^{n+2}), \quad (39)$$

$$J_n'(kr_e) = \frac{(kr_e)^{n-1}}{2^n (n-1)!} + O(\beta^{n+1}), \quad (40)$$

$$\frac{H_n^{(1)}(2kL)}{H_m^{(1)\prime}(kr_e)} = -2^{n-m} \frac{(n-1)!}{m!} \frac{(kr_e)^{m+1}}{(2kL)^n} + O(\beta^{m-n+3}), \quad (41)$$

$$\frac{H_n^{(1)}(2kL)}{H_0^{(1)\prime}(kr_e)} = -2^{n-1} \frac{(n-1)! kr_e}{(2kL)^n} + O(\beta^{3-n} \log(\beta)), \quad (42)$$

$$\frac{H_0^{(1)}(2kL)}{H_n^{(1)\prime}(kr_e)} = O(\beta^{n+1} \log(\beta)). \quad (43)$$

After tedious but simple algebra, radiation impedance, $\bar{Z}_w$, takes the following form:

$$\bar{Z}_w = -ik\delta_w, \quad (44)$$

where the outer end correction in the presence of wall δ_w is

$$\delta_w = \frac{e}{\psi} \sum_{n=1}^{\infty} \left[\frac{\psi q(n) y^n \cos(n\phi)}{4n} + b_n \frac{2e^{-in\phi} y^n + q(n)}{2n} \right.$$
$$\left. + S_{mn} \frac{q(n)}{n} \right] + \text{c.c.}, \quad (45)$$

where

$$S_{mn} = \sum_{m=1, m\neq n}^{\infty} b_m \frac{(m+n-1)!}{m!(n-1)!} y^{m+n} e^{i(n-m)\phi}. \quad (46)$$

Here, $y = r_e/2L$. The equations for coefficients b_n, where $n \geq 1$ are

$$b_n \left(1 - y^{2n} \frac{(2n-1)!}{n!(n-1)!} \right) - S_{mn} = \frac{\psi \left(2q(n) + y^n e^{in\phi} \right)}{4\pi}. \quad (47)$$

To numerically compute δ_w, Eqs. (45)–(47) have to be truncated. Substituting radiation impedance defined by Eq. (44) in characteristic equation (20) leads to the following expression for the resonance frequency of a SR in air in the presence of a wall:

$$f_w = \frac{c}{2\pi} \sqrt{\frac{e}{\pi r_i^2 (H + \delta + \delta_w)}}. \quad (48)$$

The end correction defined by Eq. (45) is longer than the free field value, δ, if the slit is facing the wall. This means that the resonance frequency of a SR is lower in this case compared to that of a SR in the free field. For instance, the resonance frequency of C1 in a free field predicted by Eq. (27) is 2913 Hz (FEM calculations result in 2970 Hz). When the resonator is placed $L = 0.01$ m away from the wall so that the opening is facing it ($\phi = 0$), using Eq. (48) the resonance frequency 2475 Hz is calculated (FEM result is 2650 Hz). However, the resonance frequency is increased as the slit is turned away from the wall for $\phi = \pi/2$, $f_w = 2917$ Hz (FEM result 2921 Hz) and for $\phi = \pi$, $f_w = 3136$ Hz (FEM result 3050 Hz). It has to be noted that in this case at 3000 Hz, $kr_e \approx 0.41$, however, $2Lk \approx 1.1$, so the assumptions that these values are much less than unity, used in derivations, are not strictly valid. However, the trend predicted by the model is correct and the resonance frequencies differ by less than 10% from those computed numerically.

C. Resonance frequency of a split ring in porous matrix

When a SR is embedded in porous material, its resonance frequency becomes dependent on the material properties. The slit radiation impedance is represented as $\bar{Z} = -ik_r \delta'$, where $\delta' = \delta$ or $\delta' = \delta_w$ depending on whether the rigid boundary is present or not, and the characteristic equation (20) is rewritten as

$$k_r^2 = \omega \frac{e}{\pi r_i^2 (H + \delta + \delta')}. \quad (49)$$

However, in a porous material, k_r is expressed as

$$k_r = \omega \sqrt{\frac{\rho_1}{\chi_1}}, \quad (50)$$

where the effective density and the bulk modulus are defined by Eqs. (1) and (3). In Fireflex (Recticel, Belgium), the characteristic frequencies involved in these equations take the following values: $\nu_b = 781$ Hz, $\nu_c = 2049$ Hz, $\nu'_b = 298$ Hz, $\nu'_c = 846$ Hz. Let us assume that the resonance

frequency of a SR is significantly higher than ν'_c. In this case, the effective bulk modulus is close to its adiabatic value and

$$k_r^2 \approx \alpha_\infty \frac{\omega_r^2}{c^2} \left(1 + \frac{2\pi\nu_b}{-i\omega_r} \sqrt{1 + \frac{-i\omega_r}{2\pi\nu_c}} \right), \tag{51}$$

where c is the sound speed in air, $\omega_r = 2\pi f_r$, and f_r is resonance frequency. Combining this with Eq. (49) gives the following equation for $W = \omega_r/(2\pi\nu_c)$:

$$W^2 + i\frac{\nu_b}{\nu_c} W \sqrt{1 - W} = \left(\frac{\bar{K}}{2\pi\nu_c} \right)^2, \tag{52}$$

where

$$\bar{K} = \frac{c}{\sqrt{\alpha_\infty}} \sqrt{\frac{e}{\pi r_i^2 (H + \delta + \delta')}}. \tag{53}$$

For Fireflex (Recticel, Belgium), $\nu_b/\nu_c \ll 1$, so Eq. (52) can be solved approximately using the method of small perturbations. After simple transformations, this gives the following expression for the resonance frequency, f_r:

$$f_r \approx \frac{1}{2\pi} \left(\bar{K} - i2\pi\nu_b \sqrt{1 - i\frac{\bar{K}}{2\pi\nu_c}} \right). \tag{54}$$

The resonance frequency is complex due to the presence of viscous losses in the porous material. Its real part is

$$\mathrm{Re}(f_r) \approx \frac{1}{2\pi} \left(\bar{K} - 2\pi\nu_b \sqrt{\frac{\sqrt{1 + \left(\frac{\bar{K}}{2\pi\nu_c} \right)^2} - 1}{2}} \right). \tag{55}$$

For a resonator embedded in an unbounded Fireflex (Recticel, Belgium) matrix $\mathrm{Re}(f_r) \approx 1721$ Hz, which is significantly lower than its resonance frequency in air.

D. Scattering by a split ring at low frequencies

To calculate SR scattering coefficients, the low frequency model developed in Krynkin *et al.*[10] is used. It implies that a SR resonator is replaced by a layered cylinder with porous matrix inside, surrounded by a layer (thickness, H) of an effective fluid. The latter has the following characteristic impedance and wavenumber [normalized by the characteristic impedance $z = \sqrt{\rho_1 \chi_1}$ and the wavenumber of the porous material; Eq. (50)]:

$$Z_l = \frac{2\pi r_i}{e}, \quad k_l = 1 + \frac{\delta + \delta_w}{H}. \tag{56}$$

The outer radius of the cylinder remains the same as that of the SR. In the calculations the SRs were placed close to a rigid boundary; for this reason, the end correction, δ_w, appears in the equation for k_l. The scattering coefficients of a multi-layered cylinder are then used in the scattering model developed by Groby *et al.*[2]

IV. PARAMETRICAL STUDY

The aim of this section is to investigate the influence of the embedded scatterer geometry on the porous layer absorption coefficient numerically and to compare the results with the scattering model described in the Sec. III. The focus is on two particular types of inclusions: the rigid cylinder and the SR.[13–15] With SRs embedded in porous matrix, three types of phenomena can be noticed. The former two are similar to those observed for the rigid inclusions. The acoustic energy is still trapped between the inclusions and the rigid backing. Bragg's interference is also noticeable at higher frequencies. The third phenomenon is the SR resonance that enhances the absorption coefficient by trapping the sound energy inside the scatterer.

A. Influence of the slit orientation

As shown in Sec. III B the slit orientation angle, $\alpha^{\{n\}}$, influences the SR resonance frequency. This will be confirmed numerically and the influence on the trapped mode frequency will be investigated. Simulations are performed by changing the orientation of the slit relative to the wall, $\alpha^{\{n\}} = [0, \pi/6, \pi/3, \pi/2, 2\pi/3, 5\pi/6, \pi]$, and searching for frequencies at which the resonance of the SR and the mode trapping occur. These frequencies are determined by the structure of the acoustic field given by the FEM result; the SR resonance corresponds to a maximum of the pressure field located inside the resonator, while at the trapped mode frequency the pressure maximum is mostly located between the inclusions and the rigid backing. Both correspond to an enhancement of the absorption coefficient [Fig. 4(b)]. The results for the SR are shown in Fig. 3, where the frequencies of inclusion resonance (solid line with stars for FEM and dots for semi-analytical results) and the resonances of the layer (dashed line for the rigid inclusion and solid line of the resonant inclusion) are plotted against $\alpha^{\{n\}}$.

The position of the absorption coefficient peak associated with the SR resonance is strongly angle dependent
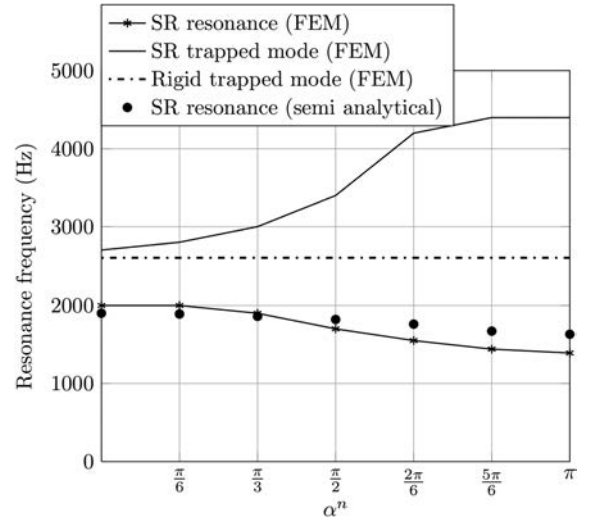

FIG. 3. Influence of SR opening orientation relative to rigid boundary on its resonance frequency in Fireflex (Recticel, Belgium). Numerical simulations are performed for $\theta^i = 0$. Dimensions of configuration C1 (see Table II).
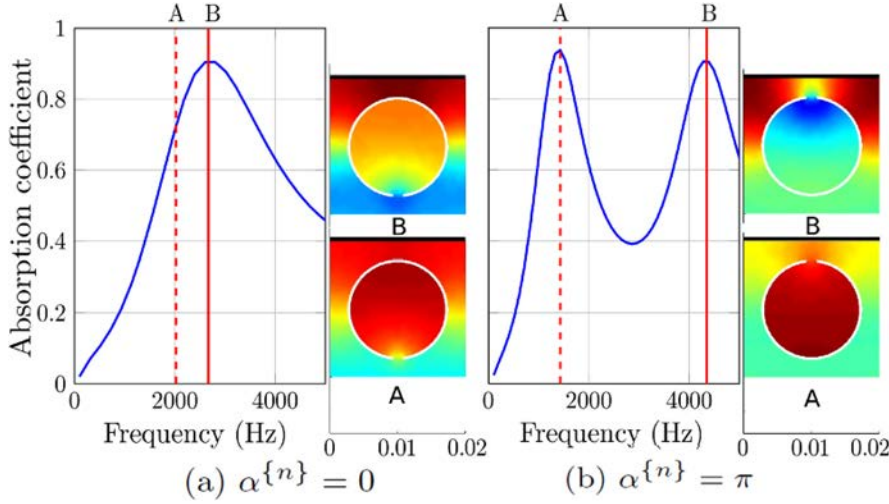
FIG. 4. (Color online) Frequency dependence of the absorption coefficient for two different orientations of the SR opening. Insets show pressure distributions near the frequency of the SR resonance (a) and the modified layer resonance (b). Dimensions of configuration C1 (see Table I).

when $\alpha^{\{n\}}$ exceeds $\pi/2$. The resonance frequency of the SR decreases and the minimum frequency is reached for $\alpha^{\{n\}} = \pi$ as expected. The frequency of the trapped mode (which corresponds to a higher frequency peak of the absorption coefficient) increases with $\alpha^{\{n\}}$. When $\alpha^{\{n\}}$ is less than $\pi/2$, the acoustic field trapped between the rigid backing and the inclusion is uniformly distributed along the axis, x_1 [see Fig. 4(a)]. When $\alpha^{\{n\}}$ exceeds $\pi/2$, the resonator introduces a periodical pressure field anomaly [see Fig. 4(b)]. With $\alpha^{\{n\}} = \pi$, the effect of this anomaly is maximum. The acoustic field is still trapped between the rigid backing and the inclusions, but the spatial distribution pattern has changed. In other words, when $\alpha^{\{n\}} \sim 0$ the trapped mode and the SR mode are coupled leading to a single absorption peak, then decoupled when $\alpha^{\{n\}}$ increases, possibly leading to the appearance of two absorption peaks.

The semi-analytical model predictions for the position of the lower frequency peak dependence on the slit orientation are in satisfactory agreement with the numerical results (Fig. 5). However, due to the low frequency nature of the model, it is unable to correctly predict the absorption coefficient behavior at higher frequencies.

The results of simulations imply that properties of the porous layer with embedded SRs could be tuned by simply changing slits orientation relative to the rigid backing. This makes the structure potentially effective for treatment of narrow frequency band noise. All the results presented so far have been obtained for a plane wave incident normally to the layer surface, i.e., $\theta^i = 0$. It is known that for a 2D sonic crystal, the absorption coefficient depends on the incidence angle because the wave does not encounter the same periodicity pattern and, hence, is not scattered in the same way for different angles.[16] A similar behavior can be expected for the structure with embedded SRs. The results of simulations (see Fig. 6) show that the absorption due to the SR resonance is not strongly influenced by the angle of incidence because the resonance frequency is independent on the way the resonator is excited. On the other hand, the trapped mode frequency and the absorption peak due to this mode increase slowly with θ^i. This phenomenon has been already observed for other types of scatterers, for instance, rigid square inclusions.[17] The trapped mode is dependent on the distance, L, between the inclusion and the rigid backing.[2] The frequency of this mode increases as L decreases. When the incident wave strikes the material at an angle, θ^i, the projection of the distance, L, on the wave vector direction is $L_{\theta^i} = L \cos \theta^i$. When $\theta^i > 0$, the distance L_{θ^i} is less than L which leads to the frequency increase.
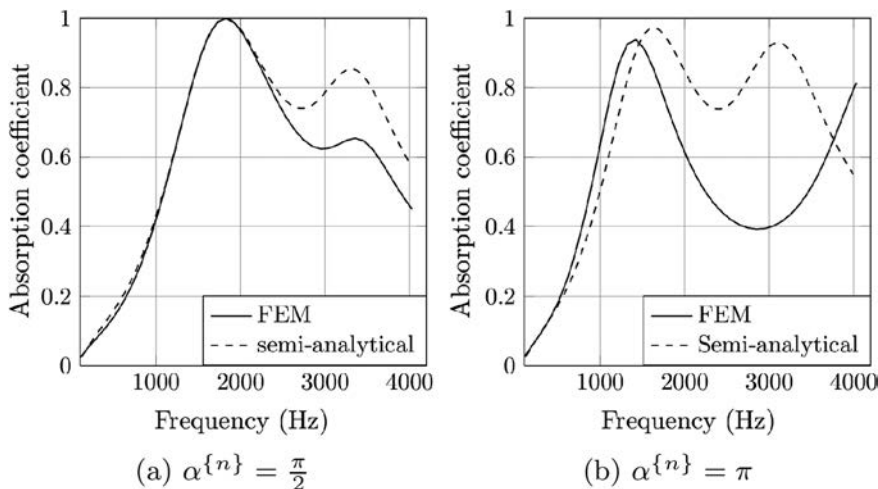

FIG. 5. Comparison between FEM and semi-analytical results for the absorption coefficient of Fireflex (Recticel, Belgium) layer with SR inclusions having slits positioned at two different angles, $\alpha^{\{n\}}$. Dimensions of configuration C1 (see Table I).
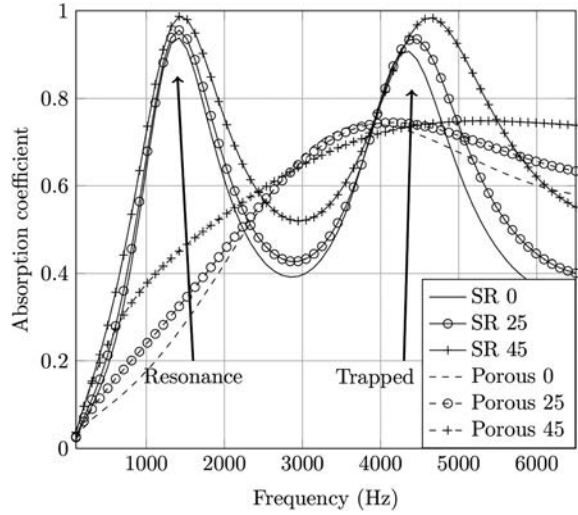
FIG. 6. Dependence of the absorption coefficient for a layer of Fireflex (Recticel, Belgium) with SR inclusions on the angle of incidence, $\alpha^{\{n\}} = \pi$. Dimensions of the configuration C1 (see Table I).

B. Creation of a "supercell" by varying the inclusion orientation

It has been shown above that the orientation of the inclusions can offer a tunability. This leads to the design of a "supercell" composed of several inclusions oriented at different angles, $\alpha^{\{n\}}$. This could widen the frequency band where high values of the absorption coefficient are achieved. Different configurations are possible, but here the focus is on a "supercell" made with two SRs.

The distance between the two inclusions is kept equal to 2 cm, but the periodicity of the structure is now $d = 4$ cm. The external radius is $r_e = 0.74$ cm. Although the positions of the SRs are the same as before, they are not oriented in the same way relative to the rigid boundary. This changes the periodicity of the anomaly and leads to different modes for the rigid backing entrapment. The cell in configuration (1) contains a single rigid inclusion (see Fig. 7). For this configuration only, the trapped mode and the Bragg's interference
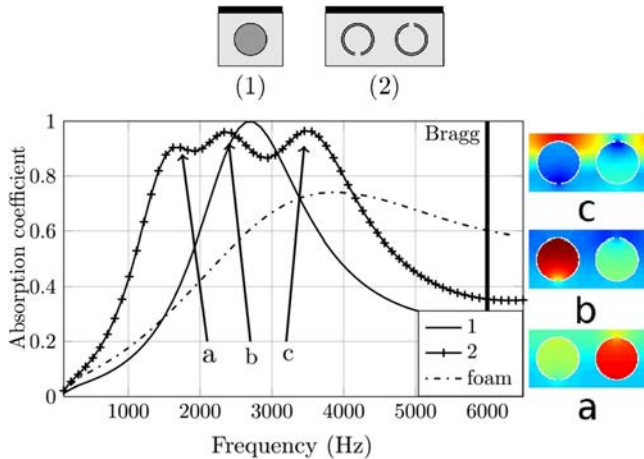
are noticeable in the considered frequency range. Comparison of the absorption coefficient for this configuration with that of a "supercell" emphasizes the advantages of the resonant inclusions. The simulations have been also performed for a "supercell" composed of four inclusions oriented with $\alpha^{\{n\}} = [\pi/2, 2\pi/3, 5\pi/6, \pi]$. However, in this case, the resonance frequencies are too close to each other resulting in a narrow frequency band of high absorption at 1500 Hz and another maximum of absorption at 4000 Hz due to the trapped mode. The configuration (2) is efficient for sound absorption in a frequency range between 1500 Hz and 3500 Hz, where the absorption coefficient value reaches 0.9. The resonances of each inclusion and the trapped mode are close enough to excite some coupled modes and to keep a large absorption coefficient value in a wide frequency band. This means that absorption coefficient value as high as 0.9 can be achieved for wavelengths ten times larger than the structure thickness, conferring the status of a metamaterial for this structure.

V. EXPERIMENTAL VALIDATION

Measurements have been performed to validate the numerical and semi-analytical models. The sample tested is composed of melamine foam as the porous matrix and hollow aluminum cylinders with and without slits as rigid inclusions (Fig. 8). Parameters of the inclusions used in measurements are summarized in Table III. The absorption coefficient of the sample is measured in an impedance tube with a square cross section with a side length 4.2 cm. The tube cut-off frequency is 4200 Hz. By assuming that plane waves propagate below the cut-off frequency, the infinitely rigid boundary conditions of the tube act like perfect mirrors and create a periodicity pattern in the x_1 and x_3 directions with a periodicity of 4.2 cm. This technique was previously used in the article by Groby *et al.*[18] and allows to determine experimentally the absorption coefficient of a quasi-infinite 2D periodic structure just with one unit cell. Two aluminum cylinders were inserted in the porous matrix to have two unit

FIG. 7. (Color online) Comparison between absorption coefficients of Fireflex (Recticel, Belgium) layer with SR inclusions arranged in a "supercell" and with rigid inclusions. Normal incidence plane wave. Dimensions of configuration C1 (see Table I).

FIG. 8. (Color online) Picture of one of the characterized samples: "supercell" of two SRs with one of them taken out.

TABLE III. Characteristic dimensions of the sample used in the experiments. These geometric values are defined Fig. 1.

C2	r_i (cm)	r_e (cm)	d (cm)	e (cm)	h (cm)	l (cm)
	0.65	0.7	4.2	0.15	2.1	1.15

cells of 2.1 cm side length in one sample. The parameters of the melamine foam are slightly different from those of Fireflex (Recticel, Belgium) and are summarized in Table IV. The sample is placed at the end of the tube against a copper plug that closes the tube and acts as a rigid boundary.

First, the FEM results are validated by comparing its results with the experimental data and the analytical model[2] predictions for a sample with rigid inclusions embedded in the porous matrix (see Fig. 9). This analytical model is based on the use of multipole method. FEM results are clearly in agreement with the analytical model and the experiments, showing a well-defined maximum of absorption coefficient in both cases. The lower frequency values of the absorption coefficient given by the FEM do not match the data exactly. The reason for this is most likely due to the defects of the real sample and of its positioning in the tube (misalignment of the inclusions with the sample faces, uncertainties on the foam parameters, uncertainties on the placement of the sample in the tube, boundaries conditions between the porous and the tube,…). The inclusions are hollow aluminum cylinders. A first measurement is made (not shown in this article) with empty inclusions where the absorption coefficient is even higher in the low frequency range. A small leak at the upper and lower boundaries of the sample allows interactions between the incident wave and the inside of the inclusion that increase the absorption coefficient. A measurement is also performed using inclusions filled with Plasticine. The experimental absorption coefficient estimation is then closer to the prediction, but is still relatively larger than the FEM value in the low frequency range. This might be due to the Plasticine that cannot be considered perfectly rigid. Measurement of the 2.1 cm thick foam, without inclusions, is also performed showing a perfect agreement with the model. These measurements are not shown here for the sake of clarity.

This problem disappears in the next experiments where the rigid inclusions are replaced by the SRs (see Figs. 10 and 11). In both experiments, the same porous matrix is used. The material inside the SRs is melamine foam, extracted when the inclusions were inserted for the first time. When $\alpha^{\{n\}} = 0$ (Fig. 10), the FEM fits perfectly to the experimental results, whereas the semi-analytical calculation captures well the tendency with an overestimation of the curve between

TABLE IV. Parameters of the porous foam (melamine) used in experiments where ϕ is the porosity, α_∞ is the tortuosity, Λ and Λ' are the characteristic viscous and thermal lengths, respectively, and σ is the material flow resistivity.

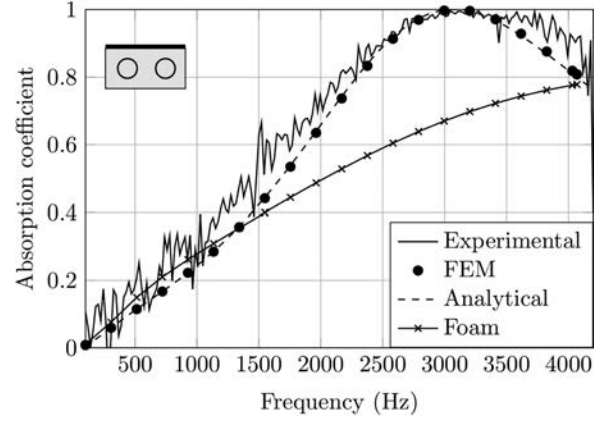| ϕ	α_∞	Λ (μm)	Λ' (μm)	σ (N s m^{-4})
0.99	1.02	160	220	11000

FIG. 9. Comparison between experimental and numerical results for the absorption coefficient of melamine layer with rigid inclusions, configuration C2. Dimensions of the sample are given in Table III.

1300 Hz and 3000 Hz. When $\alpha^{\{n\}} = \pi$ (Fig. 11), for both numerical and semi-analytical calculations, the low frequency behavior of the absorption coefficient is in agreement with experimental results whereas the higher frequency behavior is less well-captured. This can be due to a misplacement of the sample in the impedance tube that changes the spacial periodicity and so changes the experimental frequency and efficiency of the trapped mode.

By comparison with Fig. 9, the enhancement of the absorption coefficient due to SRs is clearly noticeable with its maximum appearing at $f \sim 3000$ Hz for the rigid inclusions, $f \sim 2500$ Hz for the SRs with $\alpha^{\{n\}} = 0$, and $f \sim 2000$ Hz for the SRs with $\alpha^{\{n\}} = \pi$.

A final experiment confirms the efficiency of the "supercell" described in Sec. IV B (see Fig. 12, where one of the inclusions is oriented with $\alpha^{\{n\}} = 0$ and the other with $\alpha^{\{n\}} = \pi$). The experiment and the simulations are in a good agreement. This proves the possibility of the efficient absorption of frequencies with wavelength in air 8.5 times larger than the structure thickness. The comparison with the absorption coefficient of foam with no inclusions (solid line with cross) demonstrates that even for frequencies around 500 Hz, the absorption coefficient is increased from 0.15 to 0.2, which represents 30% of improvement, and for 2000 Hz,
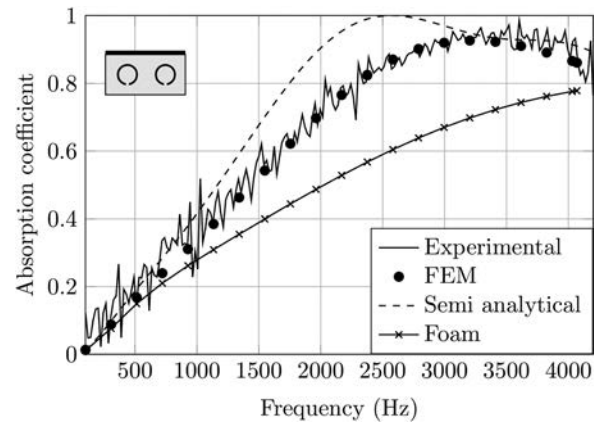

FIG. 10. Comparison between experimental and numerical results for the absorption coefficient for a sample composed of SR inclusions in a melamine layer with $\alpha^{\{n\}} = 0$. Dimensions of the sample are given in Table III.
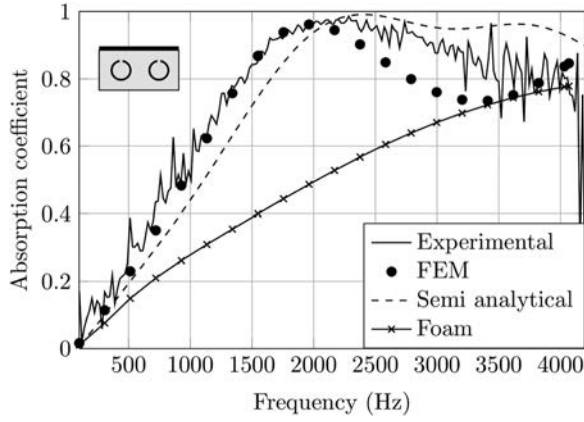
FIG. 11. Comparison between experimental and numerical results for the absorption coefficient of melamine layer with SR inclusions, configuration C2, $\alpha^{\{n\}} = \pi$. Dimensions of the sample are given in Table III.

the improvement is maximum with the absorption coefficient value increased from 0.5 to 0.9.

VI. CONCLUSION

The influence of the periodically arranged inclusions on the absorption coefficient of a rigidly backed porous layer was studied theoretically, numerically, and experimentally. In addition to the absorption features related to excitation of modified layer modes and to Bragg's interference, the structure possesses a quasi-total (close to unity) absorption peak below the quarter-wavelength resonance frequency. This occurs when one row of rigid cylindrical inclusions is embedded in a porous layer whose thickness and material properties, mainly the static flow resistivity, are correctly chosen. This particular feature enables the design of the compact sound absorbing packages and is explained by a complex trapped mode excitation, which leads to an increase of pressure gradient inside the porous layer. When resonant inclusions are embedded in the porous layer, the low frequency behavior of the absorption coefficient can be significantly changed. Near the inclusion resonance frequency, a quasi-total absorption peak occurs. For the SR inclusions in

Fireflex (Recticel, Belgium) foam, the frequency of this peak corresponds to the wavelength nearly ten times larger than the layer thickness. This suggests that the structure can be considered as an acoustic metamaterial of a special type. The resonance frequency of the inclusions depends on the orientation of slits relative to the rigid boundary (described by angle $\alpha^{\{n\}}$). The proximity of the rigid backing and the slit leads to an increase of the end correction (extended resonator neck). This phenomenon offers a possibility of a tunable absorber, which can be efficient in a wide range of frequencies. In case of more than one inclusion per spatial period, the quasi-total absorption in a wider frequency range can be obtained when the slits of the neighboring inclusions have different orientations relative to the backing. However, the characteristic dimensions of the inclusions and the layer have to be carefully chosen to make the excitation of the coupled modes possible in order to achieve high absorption coefficient values. The predictions of a semi-analytical scattering model described in this article are in satisfactory agreement with the numerical results at low frequencies (below and close to resonances). However, the model needs to be extended if the accurate predictions for higher frequencies are required. In conclusion, embedding resonant inclusions in a porous layer offers an alternative to multi-layering and double porosity materials in the design of sound absorption packages for low frequency applications.
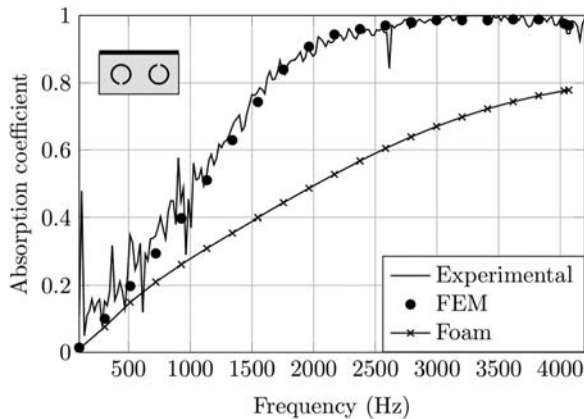
FIG. 12. Comparison between experimental and numerical results for the absorption coefficient for a sample composed of two SR inclusions in a melamine layer, configuration C2, with $\alpha^{\{n\}} = 0$ for the first SR, $\alpha^{\{n\}} = \pi$ for the second one. Dimensions of the sample are given in Table III.

[1]L. Brekhovskikh and R. Beyer, *Waves in Layered Media* (Academic, New York, 1960), Vol. 4, pp. 1–160.

[2]J. Groby, O. Dazel, A. Duclos, L. Boeckx, and L. Kelders, "Enhancing the absorption coefficient of a backed rigid frame porous layer by embedding circular periodic inclusions," J. Acoust. Soc. Am. **130**, 3771–3780 (2011).

[3]J. Groby, A. Wirgin, L. De Ryck, W. Lauriks, R. Gilbert, and Y. Xu, "Acoustic response of a rigid-frame porous medium plate with a periodic set of inclusions," J. Acoust. Soc. Am. **126**, 685–693 (2009).

[4]C. M. Linton and P. McIver, "Embedded trapped modes in water waves and acoustics," Wave Motion **45**, 16–29 (2007).

[5]R. Porter and D. Evans, "Embedded Rayleigh-Bloch surface waves along periodic rectangular arrays," Wave Motion **43**, 29–50 (2005).

[6]D. Johnson, J. Koplik, and R. Dashen, "Theory of dynamic permeability and tortuosity in fluid-saturated porous media," J. Fluid Mech. **176**, 379–402 (1987).

[7]Y. Champoux and J. Allard, "Dynamic tortuosity and bulk modulus in air-saturated porous media," J. Appl. Phys. **70**, 1975–1979 (1991).

[8]J. Allard, O. Dazel, G. Gautier, J. Groby, and W. Lauriks, "Prediction of sound reflection by corrugated porous surfaces," J. Acoust. Soc. Am. **129**, 1696–1706 (2011).

[9]A. Norris and G. Wickham, "Elastic Helmholtz resonators," J. Acoust. Soc. Am. **93**, 617–630 (1993).

[10]A. Krynkin, O. Umnova, A. Chong, S. Taherzadeh, and K. Attenborough, "Scattering by coupled resonating elements in air," J. Phys. D: Appl. Phys. **44**, 125501 (2011).

[11]E. Shenderov, *Wave Problems in Underwater Acoustics* (Sudostroenie, Leningrad, 1972), p. 126.

[12]M. Abramowitz and I. Stegun, *Handbook of Mathematical Functions: With Formulas, Graphs, and Mathematical Tables* (Dover, New York, 1964), Vol. 55, p. 363.

[13]D. P. Elford, L. Chalmers, F. V. Kusmartsev, and G. M. Swallowe, "Matryoshka locally resonant sonic crystal," J. Acoust. Soc. Am. **130**, 2746–2755 (2011).

[14]A. Movchan and S. Guenneau, "Split-ring resonators and localized modes," Phys. Rev. B **70**, 125116 (2004).

[15]V. Romero-Garca, J. Sánchez-Pérez, and L. Garcia-Raffi, "Tunable wideband bandstop acoustic filter based on two-dimensional multiphysical phenomena periodic systems," J. Appl. Phys. **110**, 014904 (2011).

[16]J. Joannopoulos, *Photonic Crystals: Molding the Flow of Light* (Princeton University Press, Princeton, NJ, 2008), Chap. 3, 5, 10, pp. 35, 44–92.

[17]B. Nennig, Y. Renou, J. Groby, and Y. Aurégan, "A mode matching approach for modeling two dimensional porous grating with infinitely rigid or soft inclusions," J. Acoust. Soc. Am. **131**, 3841–3852 (2012).

[18]J. Groby, W. Lauriks, and T. Vigran, "Total absorption peak by use of a rigid frame porous layer backed by a rigid multi-irregularities grating," J. Acoust. Soc. Am. **127**, 2865–2874 (2010).